AIAA 80-1613R

Reduced-Order Optimal Feedback Control Law Synthesis for Flutter Suppression

V. Mukhopadhyay,* J.R. Newsom,† and I. Abel‡
NASA Langley Research Center, Hampton, Va.

A method of synthesizing reduced-order optimal feedback control laws for a high-order system is developed. A nonlinear programming algorithm is employed to search for the control law design variables that minimize a performance index defined by a weighted sum of mean-square steady-state responses and control inputs. An analogy with the linear quadratic Gaussian solution is utilized to select a set of design variables and their initial values. An input-noise adjustment procedure is used in the design algorithm to improve the stability margins of the system. The method is applied to the synthesis of an active flutter-suppression control law for an aeroelastic wind tunnel wing model. The reduced-order control law is compared with the corresponding full-order control law. The study indicates that by using the present algorithm, near optimal low-order flutter suppression control laws with good stability margins can be synthesized.

Nomenclature

A = controller dynamics matrix
$[\hat{A}_n], [\hat{B}_m]$ = matrices for polynomial fit, Eq. (2)
B = controller input matrix
B_0 = Kalman filter gain matrix
C = controller output matrix
C_0 = optimal full-state feedback gain matrix
c = reference chord length
$[D_s]$ = structural damping matrix
F = plant dynamics matrix
F_a = augmented dynamics matrix
G_a = augmented noise input matrix
G_u = plant input matrix
G_w = gust input matrix
H = sensor output matrix
H_D = design output matrix
I = unity matrix
J = performance index
$[K]$ = generalized stiffness matrix
L = number of aerodynamic lag terms
M = order of controller
$[M]$ = generalized mass matrix
N_c = number of control inputs
N_D = number of design outputs
N_0 = number of outputs or sensors
N_s = number of plant states
q = dynamic pressure
q_F = flutter dynamic pressure
$[\hat{Q}], [\hat{Q}]_G$ = s-plane approximation of unsteady aerodynamics matrices
Q_a = augmented weighting matrix
Q_1 = design output symmetric weighting matrix
Q_2 = control input symmetric weighting matrix
R = key state selection matrix
R_a = augmented noise intensity matrix
R_u = fictitious input-noise intensity matrix
R_v = measurement noise intensity matrix
R_w = plant noise intensity matrix
s = Laplace variable
t = time
u = control input vector ($N_c \times 1$)
U = input covariance matrix (steady state)
V = freestream velocity
v = measurement noise vector
w = plant noise vector
x_a = augmented state vector
x_c = controller state vector ($M \times 1$)
x_s = plant state vector ($N_s \times 1$)
X_a = covariance matrix of augmented state vector (steady state)
X_s, X_c, X_{sc} = components of partitioned X_a matrix
y = measurement output vector ($N_0 \times 1$)
y_D = design output vector ($N_D \times 1$)
y_{design} = quantity evaluated at design dynamic pressure
Z = accelerometer output
β_m = aerodynamic lag
δ = control surface deflection
η = augmented noise vector
η_u = fictitious input-noise vector
Λ = Lagrange multiplier matrix
$\Lambda_s, \Lambda_c, \Lambda_{sc}$ = components of partitioned Λ matrix
ξ_F = generalized coordinate vector for flexible modes
ξ_C = generalized coordinate vector for control surface deflection
ξ_G = gust velocity vector
$(\dot{})$ = represents time derivative
$[\ ]^T$ = transpose of a matrix
$E[\ ]$ = expected value of $[\ ]$
$\text{tr}[\ ]$ = trace of a square matrix $[\ ]$

Presented as Paper 80-1613 at the AIAA Guidance and Control Conference, Danvers, Mass., Aug. 11-13, 1980; submitted Oct. 23, 1980; revision received Aug. 17, 1981. This paper is declared a work of the U.S. Government and therefore is in the public domain.

*NRC-NASA Senior Reseach Associate. Member AIAA.
†Aerospace Engineer. Member AIAA.
‡Assistant Head, MAOB, Loads and Aeroelasticity Division.

Introduction

THE state space equations describing an aeroelastic system (plant) require a large number of states to accurately represent the flexible structure, unsteady aerodynamics, and actuator dynamics.[1-3] An optimal feedback control law based on the standard linear quadratic Gaussian (LQG) solution would be of the same high order as the plant. This control law (controller) is usually very sensitive to modeling errors, has poor stability margins, and often is too complex to implement in a flight computer. A method of designing a reduced-order control law using optimization techniques which can overcome these disadvantages has recently been developed[4] and is summarized in this paper.

Reduced-order control laws have been designed using transfer function matching, modal truncation, and residualization methods.[5-7] These methods only approximate

the full-order controller and the resulting control law is no longer optimal. In the present approach, the control law is synthesized by minimizing a performance index defined by a weighted sum of mean-square steady-state responses and control inputs as in a stationary LQG analysis. However, the order of the control law is assumed to be less than the order of the plant. Gradients of the performance index with respect to the design variables of the reduced-order control law are determined by solving a pair of Lyapunov equations. Using the gradients, a nonlinear programming algorithm is utilized to search for the design variables which minimize the performance index. The basis of this reduced-order controller design procedure is described in Refs. 8 and 9 and has been applied in Ref. 10 for attitude control of a flexible spacecraft.

Two problems which arise when applying this general method are the selection of a set of design variables and their initial values which result in a stable system. In the present paper, a new systematic approach is developed to overcome both problems. The design variables of the reduced-order controller are chosen in such a manner that they are analogous to the full-state optimal feedback and Kalman estimator gain matrices. Knowledge of these full-order optimal gain matrices is utilized for choosing the initial values of the design variables. In the limit when the order of the controller is the same as the order of the plant, the algorithm provides a solution which is identical to the optimal LQG results.

In general, plants using observer based control laws exhibit poor stability margins. Recently, Doyle and Stein[11] presented an input-noise adjustment procedure to improve the stability margins of full-order LQG control laws. This method is used in the present design algorithm. Results indicate that this input-noise adjustment procedure of Doyle and Stein is capable of improving the stability margins of the system with a reduced-order control law, although the theoretical proof exists only for a full-order control law.

The present method is applied to the synthesis of active flutter-suppression control laws for an aeroelastic wind-tunnel wing model represented by a 20th-order plant. Fourth- and sixth-order control laws are obtained and compared with the corresponding full-order optimal control laws. The reduced-order control laws are found to provide near optimal performance with adequate stability margins.

Equations of Motion in State-Space Form

Plant Model

The equations of motion for an aeroelastic system can be written as[2,3]

$$([M]s^2+[D_s]s+[K])\{\xi_F\}+q[\hat{Q}]\begin{Bmatrix}\xi_F\\ \xi_C\end{Bmatrix}=q[\hat{Q}]_G\begin{Bmatrix}\xi_G\\ \dfrac{}{V}\end{Bmatrix} \tag{1}$$

where $[\hat{Q}]$ and $[\hat{Q}]_G$ are s-plane approximations of the unsteady aerodynamic forces expressed as

$$[\hat{Q}]=[\hat{A}_0]+[\hat{A}_1]\left(\frac{cs}{2V}\right)+[\hat{A}_2]\left(\frac{cs}{2V}\right)^2+\sum_{m=1}^{L}\frac{[\hat{B}_m]s}{s+(2V/c)\beta_m} \tag{2}$$

$[\hat{A}_n]$ and $[\hat{B}_m]$ are real coefficient matrices relating unsteady aerodynamics in the frequency plane to the approximating functions in the s plane. Unsteady aerodynamic forces on the wing and control surface due to sinusoidal motion and gust are generated herein using doublet lattice aerodynamics. By defining a plant state vector x_s composed of flexible modes, their time derivates, aerodynamic lag terms within the summation sign in Eq. (2), and control surface actuator states and turbulence states, the state-space model of the plant along with the output equations can be expressed[4] in the standard form as

$$\dot{x}_s=Fx_s+G_u u+G_w w \tag{3}$$

$$y=Hx_s+v \tag{4}$$

$$y_D=H_D x_s \tag{5}$$

The plant and measurement noise vectors w and v are zero mean white noise processes with intensities R_w and R_v, respectively.

Controller Model

A block diagram of the control scheme is shown in Fig. 1. The controller model is assumed to be

$$\dot{x}_c=Ax_c+By \tag{6}$$

$$u=Cx_c \tag{7}$$

where x_c represents the controller state vector of order M where $M\le N_s$. The terms A, B, and C are matrices of size $M\times M$, $M\times N_0$, $N_c\times M$, respectively. Out of the $M(M+N_0+N_c)$ elements of the A, B, and C matrices only $M(N_0+N_c)$ are independent[10] and can be chosen as free design variables. Equation (6) represents a filter which processes the output measurements before being fed back through the gain matrix C. Equations (6) and (7) represent a transfer function relation, $u=C[sI-A]^{-1}By$, which is commonly referred to as an output feedback control law.

Control Law Synthesis Method

Augmented State Equations

By defining an augmented state vector

$$x_a\equiv\begin{Bmatrix}x_s\\ \hline x_c\end{Bmatrix} \tag{8}$$

the closed-loop system is represented by

$$\begin{Bmatrix}\dot{x}_s\\ \hline \dot{x}_c\end{Bmatrix}=\left[\begin{array}{c|c}F & G_uC\\ \hline BH & A\end{array}\right]\begin{Bmatrix}x_s\\ \hline x_c\end{Bmatrix}+\left[\begin{array}{c|c}G_w & 0\\ \hline 0 & B\end{array}\right]\begin{Bmatrix}w\\ \hline v\end{Bmatrix} \tag{9}$$

or

$$\dot{x}_a=F_a x_a+G_a\eta$$

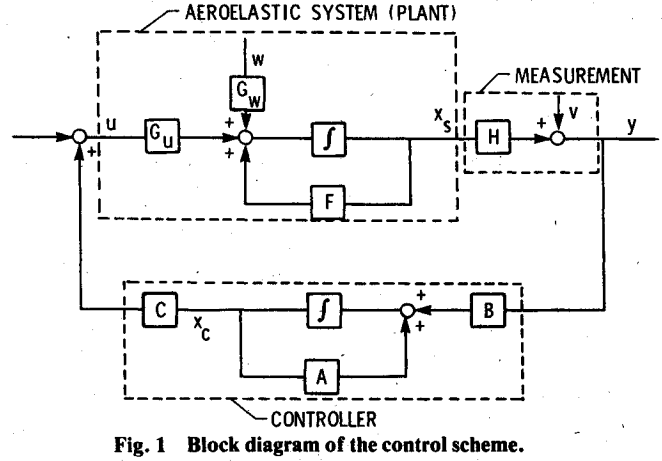

Fig. 1 Block diagram of the control scheme.

If F_a is stable with the chosen values of A, B, and C, the covariance of x_a reaches a steady-state value which satisfies the Lyapunov equation given by

$$F_a X_a + X_a F_a^T = -G_a R_a G_a^T \tag{10}$$

where

$$X_a \equiv \lim_{t\to\infty} \mathrm{E}[x_a x_a^T] \equiv \left[\begin{array}{c|c} X_s & X_{sc} \\ \hline X_{sc}^T & X_c \end{array}\right] \tag{11}$$

and

$$R_a \equiv \left[\begin{array}{c|c} R_w & 0 \\ \hline 0 & R_v \end{array}\right] \tag{12}$$

Performance Index

The control law is synthesized using a conjugate gradient algorithm[12] to search for the $M(N_0+N_c)$ design variables of the Mth-order control law [Eqs. (6) and (7)] which minimize a performance index, J, defined by

$$J \equiv \lim_{t\to\infty} \mathrm{E}[Y_D^T Q_1 Y_D + u^T Q_2 u]$$

$$= \mathrm{tr}[(H_D^T Q_1 H_D) X_s] + \mathrm{tr}[Q_2 U] \tag{13}$$

where X_s and U are steady-state covariance matrices of the states, x_s, and control inputs, u, respectively. Using Eqs. (5, 7, and11), Eq. (13) reduces to

$$J = \mathrm{tr}\left(\left[\begin{array}{c|c} H_D^T Q_1 H_D & 0 \\ \hline 0 & C^T Q_2 C \end{array}\right] \left[\begin{array}{c|c} X_s & X_{sc} \\ \hline X_{sc}^T & X_c \end{array}\right] \right)$$

$$\equiv \mathrm{tr}[Q_a X_a] \tag{14}$$

Gradients

The gradients of J with respect to the elements of the matrices, A, B, and C can be expressed as[4]

$$\frac{\partial J}{\partial A} = 2[\Lambda_{sc}^T X_{sc} + \Lambda_c X_c] \tag{15}$$

$$\frac{\partial J}{\partial B} = 2\left([\Lambda_{sc}^T X_s + \Lambda_c X_{sc}^T] H^T + \Lambda_c B R_v \right) \tag{16}$$

$$\frac{\partial J}{\partial C} = 2\left(Q_2 C X_c + G_u^T [\Lambda_s X_{sc} + \Lambda_{sc} X_c] \right) \tag{17}$$

where Λ is a $(N_s+M)\times(N_s+M)$ symmetric Lagrange multiplier matrix defined as

$$\Lambda \equiv \left[\begin{array}{c|c} \Lambda_s & \Lambda_{sc} \\ \hline \Lambda_{sc}^T & \Lambda_c \end{array}\right] \tag{18}$$

which satisfies the dual Lyapunov equation

$$F_a^T \Lambda + \Lambda F_a = -Q_a \tag{19}$$

Design Variables

There are several possible ways of selecting a set of $M(N_0+N_c)$ free design variables of the control law [Eqs. (6) and (7)]. In a canonical form of the control law, the coefficients of numerator and common denominator polynomials can be identified as the design variable set. In a block diagonal form, the real and imaginary part of the controller poles and numerator residues can be taken as the design variable set. While these representations can be incorporated into the present algorithm (to optimize an existing control law in transfer function form), they are not very general and are often inconvenient from a matrix bookkeeping point of view. Also, the initial values of the design variables can be difficult to estimate. In the present method the $M(N_0+N_c)$ elements of B and C are chosen as the free design variables and a subset of the Kalman estimator gain and full-state feedback gain matrices obtained from the LQG solution are chosen as their initial values. The justification is as follows.

With a full-order controller $(M=N_s)$, if we let $A=(F-BH+G_uC)$ and use the elements of B and C as our design variables, then it can be shown[4] that the optimized values of B and C are identical to the steady-state Kalman estimator gain and full-state feedback optimal gain matrices, respectively. The controller states x_c are identified as the asymptotic estimates of the plant states x_s. By analogy, when $M<N_s$, the low-order controller may be treated as a partial estimator of M key states denoted by Rx_s (R is a Boolean matrix of order $M\times N_s$). A full discussion of this approach and the asymptotic behavior of the estimation error is presented in Ref. 4.

Thus we initially set

$$A = R(F - B_0 H + G_u C_0) R^T \tag{20}$$

$$B = R B_0 \tag{21}$$

$$C = C_0 R^T \tag{22}$$

where M key states are chosen for estimation. The matrices B_0 and C_0 are full-order Kalman estimator and optimal state feedback gain matrices, respectively. Subsequently,

$$A = RFR^T - BHR^T + RG_u C \tag{23}$$

Since A is a function of B and C, the total gradients of J with respect to B and C are given by

$$\frac{\mathrm{d}J}{\mathrm{d}B} = \frac{\partial J}{\partial B} - \frac{\partial J}{\partial A} R H^T \tag{24}$$

$$\frac{\mathrm{d}J}{\mathrm{d}C} = \frac{\partial J}{\partial C} + (RG_u)^T \frac{\partial J}{\partial A} \tag{25}$$

Knowing the performance index J and its gradients, a conjugate-gradient-type optimization procedure[12] is utilized to minimize J. The (N_s+M)th-order Lyapunov equations are solved using a program described in Ref. 13. This process is feasible provided F_a is a stable matrix for each iteration.

Robustness Recovery Technique

Plants using full-order LQG controllers usually exhibit poor stability margins. By introducing a fictitious input noise, η_u, of intensity R_u in Eq. (7) (the noise is not included in the performance index directly) and by increasing R_u by a scalar factor, the full-order controller system loop transfer function (loop broken at u) asymptotically approaches the corresponding full-state feedback loop transfer function[11] (and hence the same stability properties). The input-noise adjustment procedure is incorporated in the present reduced-order controller design process by replacing G_w and w in Eq. (9) by $[G_u \mid G_w]$ and $\left\{\begin{smallmatrix}\eta_u \\ w\end{smallmatrix}\right\}$, respectively. Consequently, R_w in Eq. (12) is replaced by

$$\left[\begin{array}{c|c} R_u & 0 \\ \hline 0 & R_w \end{array}\right]$$

The resulting effect is an additional noise term $G_u R_u G_u^T$ in the first $N_s \times N_s$ set of the Lyapunov Eq. (10). The η_u appears as an additional noise parameter in the partial-state estimation error dynamics.[4] Although not proven theoretically, numerical results show that this input-noise adjustment

procedure is also capable of improving stability margins of the plant with a reduced-order controller. The input-noise intensity matrix R_u becomes a major design parameter in this controller synthesis technique.

Design Algorithm

The design algorithm consists of the following steps:

1) Obtain B_0 and C_0 from the LQG solution.
2) Select M key states (R matrix).
3) Compute RFR^T, RG_u, HR^T, $B=RB_0$, $C=C_0R^T$.
4) Set $A=RFR^T-BHR^T+RG_uC$.
5) Test F_a for stability.
6) If F_a is stable solve Lyapunov Eqs. (10) and (19) for X_a and Λ.
7) Compute J, dJ/dB, dJ/dC.
8) Obtain the next set of B and C by a conjugate gradient algorithm.
9) Repeat steps 4-8 with new values of B and C until J converges to a minimum value.

In step 2, it is often convenient to transform the plant state equations to a block diagonal form (provided F has no repeated eigenvalues) for easier selection of key states to be estimated. In step 5, if F_a is initially unstable, then either select a new set of states and weighting matrices or increase the number of key states and start from step 1 until a stable F_a is obtained. If F_a becomes unstable during a linear search in the optimization process, the algorithm automatically searches in a new direction from the last stable solution.

Application To Flutter Suppression

Model Description

The control law synthesis method is applied to the synthesis of an active flutter-suppression control law for an aeroelastic wind tunnel model (see Ref. 1). The cantilever wing model geometry along with the control surface and sensor (accelerometer) locations are shown in Fig. 2. The state-space equations are derived using five flexible modes and two aerodynamic lag terms ($L=2$, $\beta_1=0.225$, $\beta_2=0.5$). All structural damping is assumed to be zero. For simplicity, the actuator and turbulence dynamics are neglected but their inclusion is straightforward.[4] The resulting plant model is a single-input single-output system of order 20. The open-loop dynamic pressure root locus at Mach 0.9 is shown in Fig. 3. The flutter dynamic pressure is 4.7 kPa. The control law design point is chosen to be a dynamic pressure of 7.66 kPa at Mach 0.9.

Full-Order Control Law

For comparison purposes, the full-order control law, which is identical to the LQG solution, is obtained first. The design output matrix H_D is chosen to be the same as sensor output matrix H. For this single-input single-output system the weighting and noise intensity matrices are scalars and are selected to be $Q_1=0.0001$, $Q_2=50{,}000$, $R_w=1.0\times10^{-8}$, $R_v=1.0$. The choice of Q_1 and Q_2 has the effect of nearly reflecting the unstable pole about the imaginary axis without affecting the stable poles. The noise intensities are chosen to keep the right-hand-side terms in the Lyapunov equation (10) of roughly the same order of magnitude as the left-hand-side terms. The control laws are designed at three values of R_u, namely, 0.0, 0.00001, and 0.0001. To determine the improvements in the control law designed with increasing R_u, the phase and gain margins of the plant plus the control law are determined. The Nyquist diagram of the plant with the full-order output feedback control law, presented in Fig. 4, shows a progressive increase in phase and gain margins. As predicted,[11] the Nyquist diagram aysmptotically approaches the full-state feedback result, which is a circle of unit radius centered at $(-1.0, 0.0)$. The price paid is an increase in the optimal design performance index J and associated increases in rms values of the input and output (Table 1). The closed-loop dynamic pressure root locus using the full-order control law designed with $R_u=0.0001$ (Fig. 5) shows a flutter dynamic pressure increase to 10.5 kPa.

Fourth-Order Control Law

Fourth-order control laws are synthesized by selecting the first two flexible modes and their time derivatives as the four key states. The initial values of the gain matrices B and C are obtained from the full-order solution.

In transfer function form, the control laws for $R_u=0$, 0.00001, and 0.0001 are

$$\frac{u}{y}=\frac{(-0.0765)(s-93)(s^2+68s+5732)}{(s+86)(s+1398)(s^2+9.5s+3475)} \tag{26}$$

$$\frac{u}{y}=\frac{(-0.1262)(s-56)(s^2+85s+5392)}{(s+72)(s+2192)(s^2+13s+3457)} \tag{27}$$

$$\frac{u}{y}=\frac{(-0.1157)(s-39)(s^2+70s+5588)}{(s+76)(s+2312)(s^2+14s+3472)} \tag{28}$$

respectively. Figure 6 shows a typical convergence pattern of the performance index obtained in the course of synthesizing the control law (28). The optimized J is within 11% of the full-order value. The Nyquist diagrams of the plant plus fourth-order controllers given by Eqs. (26-28) are presented in Fig. 7. With the control law designed without input noise [Eq. (26)], the stability margins are poor and relatively unaffected by controller order reduction. Although theoretically proven

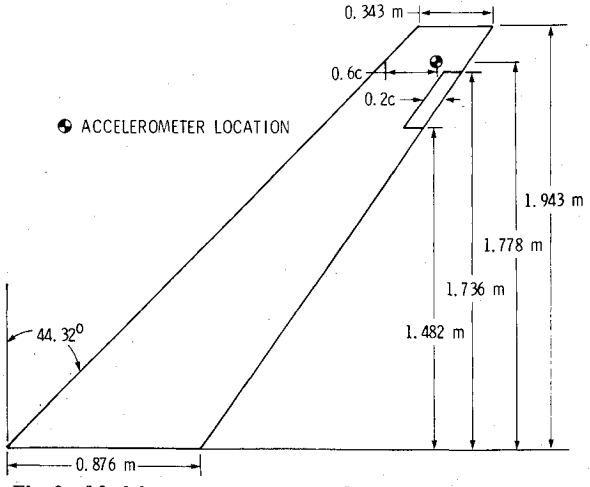

Fig. 2 Model geometry, sensor, and control surface location.

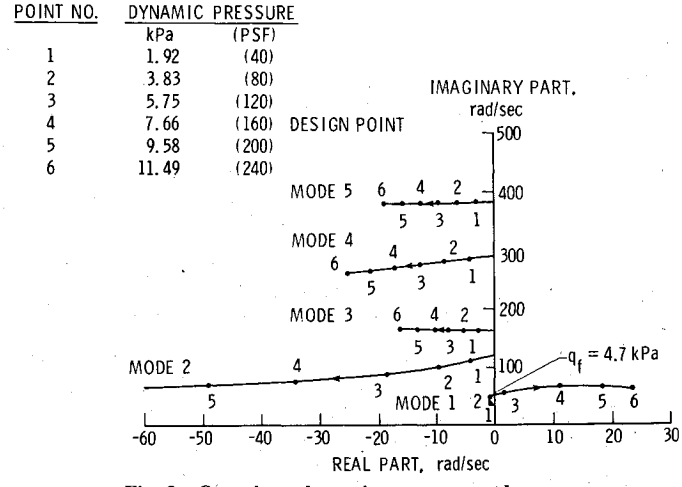

Fig. 3 Open-loop dynamic pressure root locus.

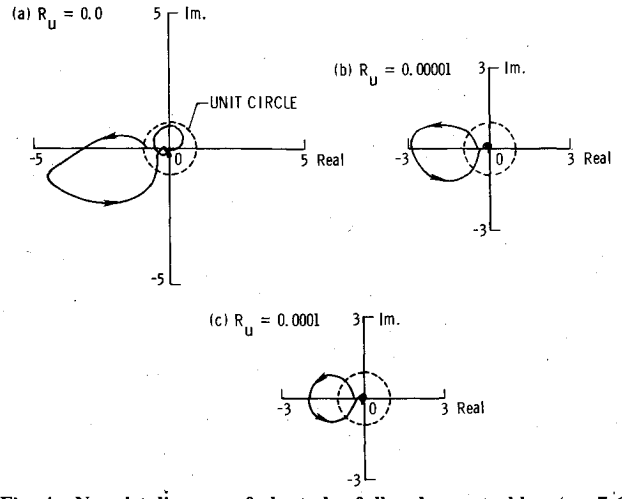

Fig. 4 Nyquist diagram of plant plus full-order control law ($q = 7.66$ kPa).

POINT NO.	DYNAMIC PRESSURE kPa	(PSF)
1	1.92	(40)
2	3.83	(80)
3	5.75	(120)
4	7.66	(160)
5	9.58	(200)
6	11.49	(240)

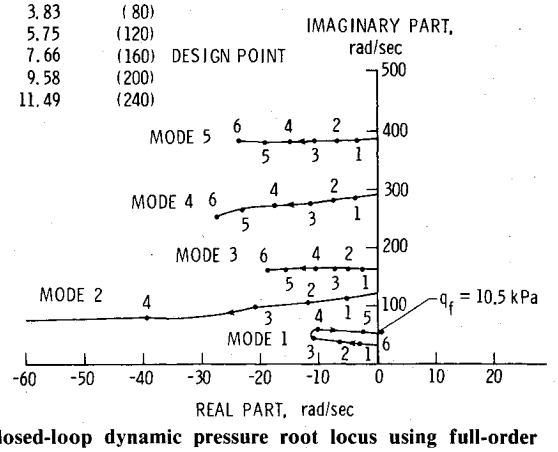

Fig. 5 Closed-loop dynamic pressure root locus using full-order control law ($R_u = 0.0001$).

Table 1 Summary of results (20th-order plant)[a]

Order of controller, m	Input noise intensity, R_u	δ_{rms}, deg	$\ddot{Z}_{rms}$, m/s^2	Performance index, J	Gain margin, db	Gain margin, rad/s	Gain margin, dB	Gain margin, rad/s	Phase margin, deg	Phase margin, rad/s	Phase margin, deg	Phase margin, rad/s	Flutter dynamic pressure, kPa
20	0	2.42	7.8	99.2	−10.0	52.0	5.2	399	14.4	20.6	60.6	101	...
20	1×10^{-5}	3.10	13.1	173.1	−9.3	60.8	13.5	320	−36.4	36.3	52.0	92	...
20	1×10^{-4}	5.42	30.5	592.0	−6.2	61.0	13.4	242	−64.0	44.0	50.0	83	10.5
4	0	2.49	8.5	105.4	−7.3	49.5	6.0	161	−15.0	21.9	65.0	93	...
4	1×10^{-5}	3.20	13.9	185.8	−10.5	57.0	5.2	157	−27.0	34.0	47.0	96	...
4	1×10^{-4}	5.68	32.7	657.1	−6.0	62.0	7.3	157	−39.0	45.0	45.0	80	10.3
6	0	2.48	8.4	104.6	−8.2	51.5	6.2	164	−16.0	21.0	63.5	91	...
6	1×10^{-5}	3.15	13.7	180.1	−8.9	61.0	5.0	161	−33.5	37.0	54.0	87	...
6	1×10^{-4}	5.56	32.2	630.6	−6.4	61.0	6.1	160	−38.0	44.8	47.0	80	10.3

[a] $H_D = H$, $Q_1 = 0.0001$, $Q_2 = 50{,}000$, $R_w = 1\times10^{-8}$, $R_v = 1.0$, $q = 7.66$ kPa.

only for a *full*-order controller, it is interesting to note that the input-noise adjustment procedure[11] is also capable of improving the phase and gain margins for a *reduced*-order controller. For a given R_u, the reduction of the controller from full to fourth order results in only a slight degradation (increase) in the optimal design performance index J (Table 1). The closed-loop dynamic pressure root locus using the fourth-order optimized control law designed with $R_u = 0.0001$ [Eq. (28)] shows (Fig. 8) a flutter dynamic pressure increase to 10.3 kPa. The corresponding Bode plot (Fig. 9a) indicates a large high-frequency response at the fifth flexible mode natural frequency (385 rad/s). This response can be reduced by a sixth-order control law designed using two additional key states representing the fifth flexible mode and its time derivative.

Sixth-Order Control

In transfer function form the resulting sixth-order control laws for $R_u = 0$, 0.00001, and 0.0001 are given by

$$\frac{u}{y} = \frac{(-0.2495)(s-83)(s^2+68s+7040)(s^2+22s+146{,}000)}{(s+114)(s+3267)(s^2+11s+3600)(s^2+24s+163{,}800)} \quad (29)$$

$$\frac{u}{y} = \frac{(-0.2526)(s-47)(s^2+70s+7200)(s^2+7s+147{,}800)}{(s+177)(s+1083)(s^2+14s+3434)(s^2+187s+325{,}600)} \quad (30)$$

$$\frac{u}{y} = \frac{(-0.4197)(s-37)(s^2+65s+6720)(s^2+2.5s+152{,}400)}{(s+161)(s+2883)(s^2+14s+3500)(s^2+276s+255{,}500)} \quad (31)$$

respectively. The Bode plot of the plant plus the control law designed with $R_u = 0.0001$ [Eq. (31)] indicate (Fig. 9b) a significant reduction of the large response near 385 rad/s. The convergence pattern of the performance index obtained while synthesizing this control law is shown in Fig. 6. The optimized J is within 6.3% of the full-order value. The Nyquist diagrams of the plant plus sixth-order controllers given by Eqs. (29-31) indicate progressive improvement in stability margins (see Fig. 10). The closed-loop dynamic pressure root locus using the sixth-order optimized control law of Eq. (31) (see Fig. 11), indicates a flutter dynamic pressure increase to 10.3 kPa. The performance index and responses are slightly lower than those with the fourth-order controller (Table 1).

To examine the performance with this control law [Eq. (31)] at off-design dynamic pressures, the system response and stability margins are computed over a range of dynamic pressures. Figure 12 shows the ratio of control deflection and acceleration to their values at the design condition plotted against dynamic pressure. The ratios decrease monotonically with reduction in dynamic pressure. Figure 13 presents the stability margins as a function of dynamic pressure. This figure indicates that a ±6 dB gain margin and a ±30 deg phase margin are maintained up to the design dynamic pressure.

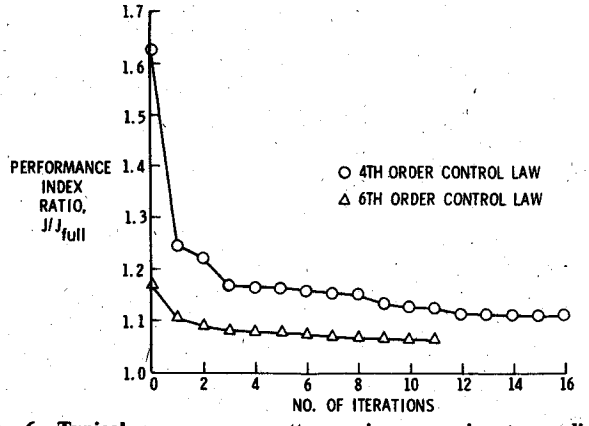

Fig. 6 Typical convergence pattern using a conjugate gradient algorithm ($R_u = 0.0001$).

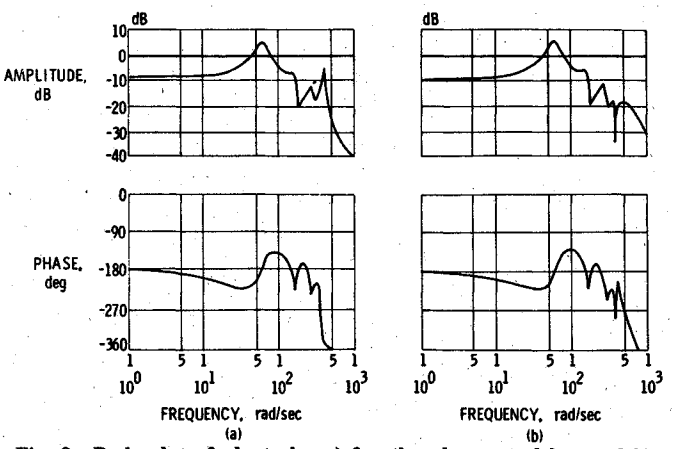

Fig. 9 Bode plot of plant plus a) fourth-order control law and b) sixth-order control law at 7.66 kPa ($R_u = 0.0001$).

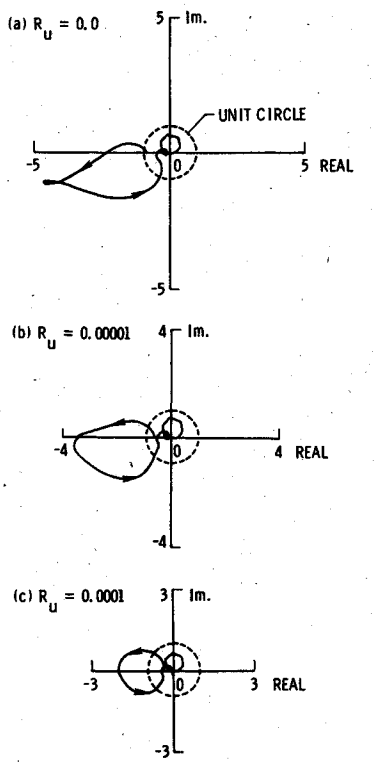

Fig. 7 Nyquist diagram of plant plus fourth-order control law ($q = 7.66$ kPa).

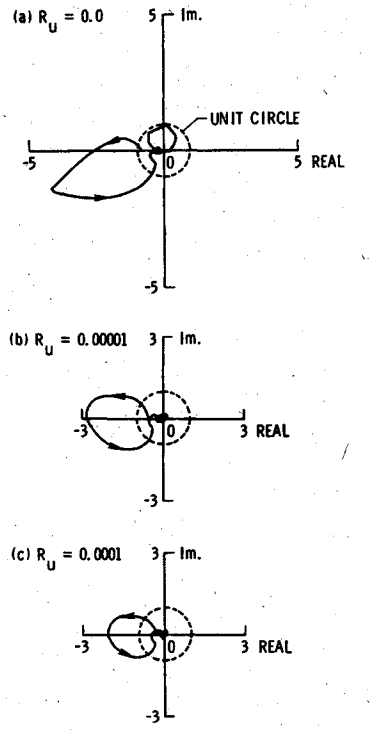

Fig. 10 Nyquist diagram of plant plus sixth-order control law ($q = 7.66$ kPa).

POINT NO.	DYNAMIC PRESSURE kPa	(PSF)
1	1.92	(40)
2	3.83	(80)
3	5.75	(120)
4	7.66	(160)
5	9.58	(200)
6	11.49	(240)

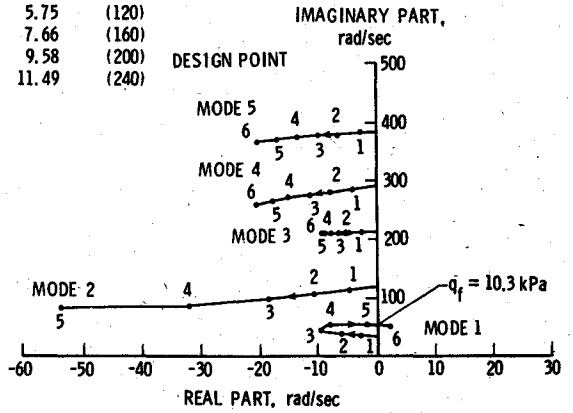

Fig. 8 Closed-loop dynamic pressure root locus using fourth-order control law ($R_u = 0.0001$).

POINT NO.	DYNAMIC PRESSURE kPa	(PSF)
1	1.92	(40)
2	3.83	(80)
3	5.75	(120)
4	7.66	(160)
5	9.58	(200)
6	11.49	(240)

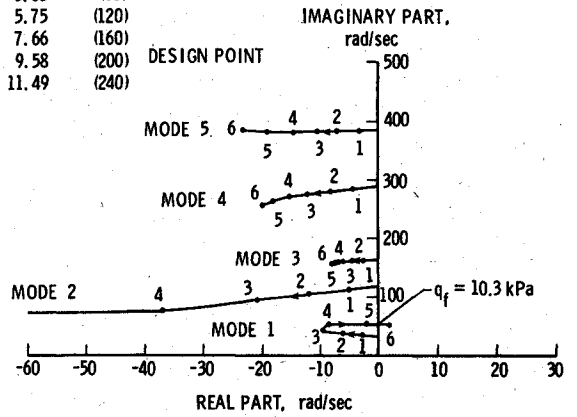

Fig. 11 Closed-loop dynamic pressure root locus using sixth-order control law ($R_u = 0.0001$).

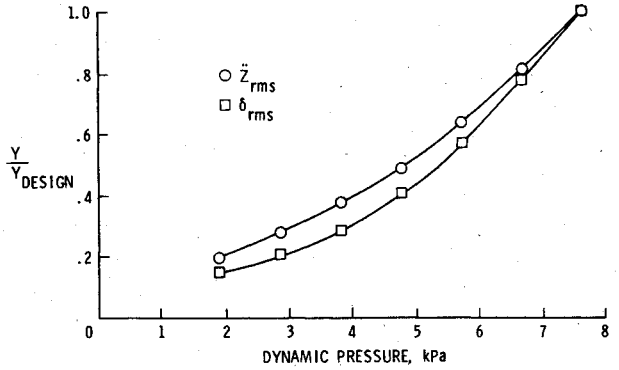

Fig. 12 Variation of response with dynamic pressure (sixth-order control law).

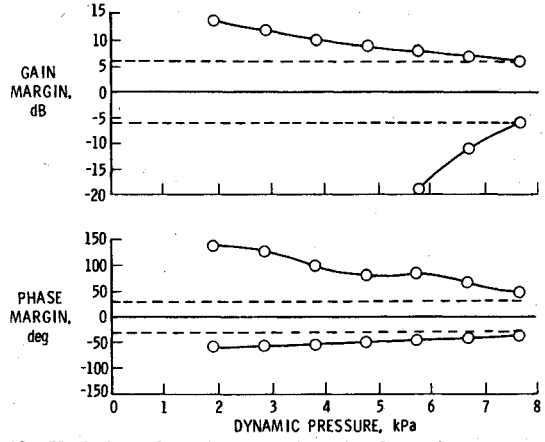

Fig. 13 Variation of stability margins with dynamic pressure (sixth-order control law).

Conclusions

A method of synthesizing reduced-order optimal feedback control laws for a high-order system is developed. A design algorithm which employs a nonlinear programming technique and utilizes an analogy with the linear quadratic Gaussian solution is presented. An input-noise adjustment procedure is used to improve the stability margins of the system. This general method is applied to the synthesis of an active flutter-suppression control law for an aeroelastic wind tunnel wing model. The important results of this study are the following.

1) The present method can be used to synthesize optimal reduced-order robust feedback control laws for a high-order plant without reducing the plant model order. However, existence of a reduced-order controller cannot be guaranteed.

2) The method is feasible provided one can find a set of key states and weighting matrices which result in a stable augmented dynamics matrix F_a.

3) Application of this method to a 20th-order plant representing an aeroelastic wing model provides fourth- and sixth-order flutter-suppression control laws which significantly increase the analytical flutter dynamic pressure. The closed-loop system performs well at off-design dynamic pressures, demonstrating its insensitivity to this parameter.

4) The numerical results indicate that the input-noise adjustment procedure of Doyle and Stein is capable of improving the stability margins of the system with a *reduced*-order controller, although the theoretical proof exists only for a *full*-order controller.

Acknowledgments

The financial support for the first author by the NASA-National Research Council Resident Research Associateship is gratefully acknowledged.

References

[1] Abel, I., Newsom, J.R., and Dunn, H.J., "Application of Two Synthesis Methods for Active Flutter Suppression on an Aeroelastic Wind-Tunnel Model," AIAA Paper 79-1633, Aug. 1979.

[2] Abel, I., "An Analytical Technique for Predicting the Characteristics of a Flexible Wing Equipped with an Active Flutter Suppression System and Comparison with Wind Tunnel Data," NASA TP-1367, Feb. 1979.

[3] Roger, K.L., "Airplane Math Modeling Methods for Active Control Design: Structural Aspects of Active Controls," AGARD-CP-228, Aug. 1977, pp. 4.1-4.11.

[4] Mukhopadhyay, V., Newsom, J.R., and Abel, I., "A Method for Obtaining Reduced Order Control Laws for High Order Systems Using Optimization Techniques," NASA TP-1876, Aug. 1981.

[5] Newsom, J.R., "A Method for Obtaining Practical Flutter Suppression Control Laws Using Results of Optimal Control Theory," NASA TP-1471, Aug. 1979.

[6] Gangsaas, D. and Ly, U.L., "Application of Modified Linear Quadratic Gaussian Design to Active Control of a Transport Airplane," AIAA Paper 79-1746, Aug. 1979.

[7] Mahesh, J.K., Stone, C.R., Garrad, W.L., and Hausman, P.D., "Active Flutter Control for Flexible Vehicles," NASA CR-159160. Vol. 1, Nov. 1979.

[8] Kwakernaak, K. and Sivan, R., *Linear Optimal Control System,* John Wiley and Sons, New York, 1972, pp. 427-434.

[9] Levine, W.S., Johnson, T.L., and Athans, M., "Optimal Limited State Variable Feedback Controllers for Linear Systems," *IEEE Transactions on Automatic Control,* Vol. AC-16, Dec. 1971, pp. 785-793.

[10] Martin, G.D. and Bryson, A.E. Jr., "Attitude Control of a Flexible Spacecraft," AIAA Paper 78-1281, Aug. 1978.

[11] Doyle, J.C. and Stein, G., "Robustness with Observers," *IEEE Transactions on Automatic Control,* Vol. AC-24, Aug. 1979, pp. 607-611.

[12] Vanderplaats, , G.N., "CONMIN—A FORTRAN Program for Constrained Function Minimization – User Manual," NASA TM X-62282, Aug. 1973.

[13] Armstrong, E.S., *ORACLS—A Design System for Linear Multivariable Control,* Marcel Dekker, Inc., New York, 1980.